AD_____

Award Number: DAMD17-02-1-0518

TITLE: Investigation of post-patient tapered monolithic optics for mammography

PRINCIPAL INVESTIGATOR: Noor Mail, Ph.D.

CONTRACTING ORGANIZATION: State University of New York - Albany
Albany, New York 12222

REPORT DATE: June 2004

TYPE OF REPORT: Annual Summary

PREPARED FOR: U.S. Army Medical Research and Materiel Command
Fort Detrick, Maryland 21702-5012

DISTRIBUTION STATEMENT: Approved for Public Release;
Distribution Unlimited

REPORT DOCUMENTATION PAGE

Form Approved
OMB No. 074-0188

1. AGENCY USE ONLY (Leave blank)	2. REPORT DATE	3. REPORT TYPE AND DATES COVERED
	June 2004	Annual Summary (1 Jun 03 - 31 May 04)

4. TITLE AND SUBTITLE
Investigation of post-patient tapered monolithic optics for mammography

5. FUNDING NUMBERS
DAMD17-02-1-0518

6. AUTHOR(S)

Noor Mail, Ph.D.

7. PERFORMING ORGANIZATION NAME(S) AND ADDRESS(ES)

State University of New York - Albany
Albany, New York 12222

E-Mail: nm7075@albany.edu

8. PERFORMING ORGANIZATION REPORT NUMBER

9. SPONSORING / MONITORING AGENCY NAME(S) AND ADDRESS(ES)

U.S. Army Medical Research and Materiel Command
Fort Detrick, Maryland 21702-5012

10. SPONSORING / MONITORING AGENCY REPORT NUMBER

11. SUPPLEMENTARY NOTES

12a. DISTRIBUTION / AVAILABILITY STATEMENT
Approved for Public Release; Distribution Unlimited

12b. DISTRIBUTION CODE

13. ABSTRACT (Maximum 200 Words)

Polycapillary x-ray optics, arrays of hollow capillary tubes used to guide x rays by total reflectance, have been shown to have potential in medical imaging at mammographic energies. Placing these optics after the object to be imaged provides very efficient rejection of Compton scatter because of the low angular acceptance of the capillaries. A Polycapillary tapered optic produced reduction in scatter fraction of a factor of 5 at 27 keV and 3 at 45 keV for a 53 mm thick polymethyl methacrylate phantom. The contrast enhancement was a factor of 2 at 27 keV and 1.5 at 45 keV. The scatter fraction and contrast data performed with energy sensitive and imaging detectors were in good agreement. A detailed calculation for comparing these broadband and monoenergenic-input scatter fraction data was performed. The agreement provides an innovative new way to predict the effect of input spectrum on contrast of an image at different energies. The PI also participated, as part of his training, in a variety of other imaging measurements at mammographic energies, including the use of DCC optics.

14. SUBJECT TERMS
None provided

15. NUMBER OF PAGES
10

16. PRICE CODE

17. SECURITY CLASSIFICATION OF REPORT	18. SECURITY CLASSIFICATION OF THIS PAGE	19. SECURITY CLASSIFICATION OF ABSTRACT	20. LIMITATION OF ABSTRACT
Unclassified	Unclassified	Unclassified	Unlimited

Table of Contents

Cover.....1

SF 298.....2

Introduction.....3

Body.....4

Key Research Accomplishments.....9

Reportable Outcomes.....9

Conclusions.....9

References.....9

Appendices.....

Scattered radiation is a major source of image degradation in x-ray imaging. The use of polycapillary tapered optics has significant potential to minimize the scattered radiation, because of the low angular acceptance of the capillaries.

The previous postdoctoral PI accepted a permanent breast cancer research position shortly after the previous annual report in June. Her measurements had included the University of Wisconsin segments of this project. The new PI started the first task for the second year at the University at Albany, physics department in December 2003. The new PI needed single taper experience. The performance of individual taper in multiple-taper optic was investigated. The tapered optics were used to perform scatter fraction and contrast measurements on polymethyl methacrylate (PMMA) phantom at 20-45 keV. The data was taken with both energy sensitive and with imaging detectors, in order to assess the effect of differing input spectra. The scatter fraction and contrast data performed with energy sensitive and imaging detectors were in good agreement. A detailed calculation for comparing these broadband and monoenergenic-input scatter fraction data was performed. The agreement provides an innovative new way to predict the effect of input spectrum on contrast of an image at different energies. Additional measurements on the full multiple taper optic will follow.

The PI also, as part of training experience with imaging systems, participated in an experiment, in collaboration with an optics manufacturer, to investigate the imaging potential of curved crystal optics. The measurements, when completed, may show promising results, and have given additional, varied, experience.

Body:

Task 1. Investigate tapered monolithic optic performance

1. Transmission as a function energy

The schematic diagram for the experimental setup is shown in Figure 1. The tapered optic, which was 17 cm long, 2.5 mm in diameter at input and 4 mm diameter at output, was placed at the focal distance which was 300 mm from the source. The capillary channels in the optic were 10 μm in diameter and the fractional open area was 50%. The optic and source were each mounted on three translation stages. The source was moved along the horizontal and vertical directions, transverse to the x ray beam to optimize the counts. A resultant source scan at 18 keV is shown in Figure 2.

The source scan curve is symmetric, which indicates no x ray leakage around the optic. Since the photons are transported through the fibers by total external reflection, the transmission efficiency is very sensitive to the incident angle. The transmission quickly drops as the source is moved off axis, shown by the transverse source scan. Transmission performance of the tapered optic at different photon energies with the source fixed at the focal point is shown in Figure 3. The transmission drops off rapidly with energy due to the drop in critical angles at higher energies. The transmission drops from 45 % to 32 % as the energy increases from 18 keV to 45 keV.

2. Uniformity

The output uniformity of the tapered optic was measured with the source at the focal distance. An image plate was placed near the optic output end, and was exposed for 20 seconds at 25kV and 0.1 mA. The rms variation of the output intensity is 6 %, which is a very good uniformity for medical imaging application.

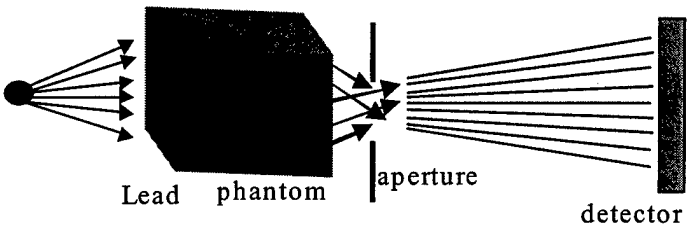

Figure 1. A schematic diagram of the experimental setup used for the scatter rejection measurement.

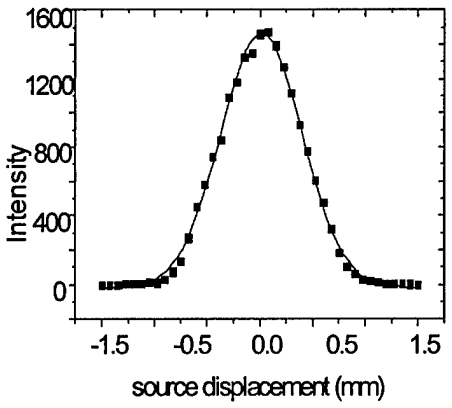

Figure 2. Optic scan for source to optic position 25 cm at photon energy 18 keV

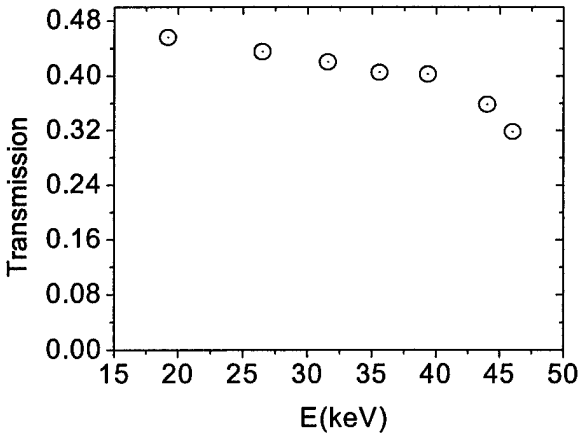

Figure 3. Transmission versus photon energy at focal distance, 31 cm.

3. Method of energy sensitive scatter fraction and contrast measurements

The phantom, mounted on two translation stages, was placed between the source and optic, 240 mm away from the source and 5 mm from the optic. For the scatter fraction measurement, lead strips with different widths, from 2.5 to 5.5 mm, but with the same thickness, were attached to the polymethyl methacrylate phantom on the side facing the source. The lead strips on the phantom were aligned sequentially with the optic input to block the direct beam. A 4 mm diameter aperture in a lead sheet was used to prevent leakage around the optic. A high purity germanium, HPGe, detector with an energy resolution of 340 eV and 580 eV at 5.9 and 122 keV, respectively, was used in this measurement. The spectra of the scattered photons, with the detector aligned behind the lead strip or near the lead strip, were recorded. The x-ray generator used in the experiment was a low current Micro Focus MS50 with an 80 μm spot size, tungsten target, and a maximum operating voltage of 100 kV. Three holes with different depths were made in a 54 mm thick polymethyl methacrylate (PMMA) phantom. A schematic diagram of the phantom is shown in Figure. The spectra for a drilled hole and the neighboring area were recorded with the energy sensitive detector. The contrast was taken as[1]

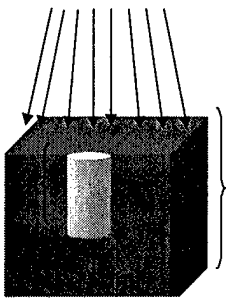

Figure 4. A schematic diagram of the phantom design for contrast measurements.

$$C = \ln\left(\frac{I_o + I_S}{I_p + I_S}\right) \qquad (1)$$

where I_o+I_S is the intensity behind the object, and I_p+I_S is the intensity for a neighboring area.

4. Method of imaging detector scatter fraction and contrast measurements

The experimental setup for the measurements with the imaging detector was the same as for the energy sensitive measurement except that the HPGe detector was replaced with a Fuji base-1800 image plate computed radiography detector, with a spatial resolution of 50 μm. Energy discrimination was obtained with the image plate by changing the tube potential and filter thickness to produce a selected energy spectrum. Images were taken with the Fuji plate with and without the optic, and read with the Fuji software.

5. Results

A. Energy sensitive detector measurements

I. Scatter fraction with energy sensitive detector

The spectra of the scattered photons with the detector aligned behind the strip, and near the strip, were recorded. For each energy window, the ratio of these intensities was plotted as a function of the width of lead strip, as shown in Figure 5 for 40 keV. The extrapolation of the linear fit to zero strip width was taken as the scatter fraction. The tube voltage was kept at 50 keV and 1 keV wide energy windows were selected on the multi-channel analyzer. The energies given in this section are the detected photon energies, for a broad input spectrum from 27 to 46 keV. The measured scatter fraction with and without the optic for the polymethyl methacrylate (PMMA) phantom at five different energies is listed in Table I. More low energy photons

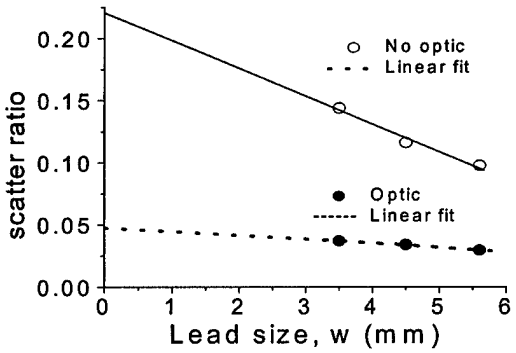

Figure 5. Scatter ratio versus lead strip width, with and without the optic for detected photons near 40 keV, using the PMMA phantom.

are scattered than are those at high energy, so the scatter fraction decreases with detected photon energy. The optic reduces the scatter more effectively low energy photons. The scatter fraction was reduced by the optic by a factor of 5 compared to the no optic case at 27 keV and by a factor of 3 at 46 keV. The expected scatter fraction of the phantom can be calculated as

$$SF = \frac{1 - e^{-\alpha_s t}}{1 - e^{-\alpha_s t}(1 - \frac{4\pi X^2}{A_p})} \qquad (2)$$

where t is the thickness of the phantom, A_P is the area, X is the apparent source position, and α_s is the scatter attenuation coefficient of the phantom material. Five different values of apparent scatter source position were found by fitting the data for the five different energies. The values of the apparent source location, plotted in Figure 6, increase as the detected photon energy rises closer to the maximum given by the tube voltage, since these photons have undergone less scattering. Similarly the fraction of scattered photons decreases as the detected photon energy rises. The scatter fraction with the optic is calculated

Photon E, keV	SF without	SF withoptic	
	Measured	Measured	Calculated
27	0.42 ± 0.05	0.08 ± 0.01	0.10
30	0.32 ± 0.05	0.07 ± 0.01	0.07
35	0.25 ± 0.07	0.06 ± 0.01	0.07
40	0.21 ± 0.06	0.05 ± 0.01	0.06
46	0.20 ± 0.04	0.05 ± 0.01	0.06

Table I. Measured and calculated SF with and without the optic at five different energies.

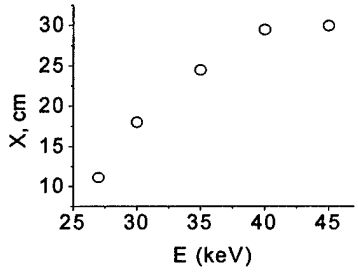

Figure 6. Apparent scatter source position, X, versus detected photon energy. An X of 30 cm would indicate isotropic scatter, centered from the center of the phantom.

$$SF^{op} = \frac{T_s SF}{T_p(1 - SF) + T_s SF} \qquad (3)$$

using the measured scatter fraction without the optic, the measured primary transmission of the optic, and a scatter transmission of the optic given by

$$T_S = e^{-L(1-f)\mu\rho} \qquad (4)$$

where L is the length of the optic, f is the fractional open area, μ is the attenuation coefficient of the optic and ρ is the density. The calculated scatter fraction with the optic agrees well with the measurement.

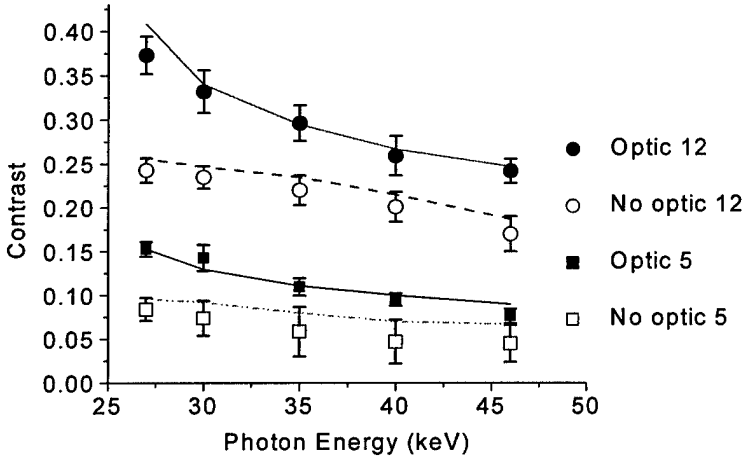

Figure 7. Contrast versus detected photon energy for hole of 5 and 12 mm depths. Solid and dotted lines are calculations for the optic and no optic case, respectively.

II. Contrast with energy sensitive detector

Measured and calculated contrasts with and without the optic for two different hole depths as a function of detected photon energy are shown in Figure 6. As expected, the contrast decreases with increasing photon energy, and increases with increasing the hole depth. The contrast in the presence of scatter was calculated as

$$C_S = \ln\left((1-SF)e^{\alpha_T d} + SF\right), \quad (5)$$

where α_T is total attenuation coefficient, d is the hole depth, and SF is the measured scatter fraction from Table I. The measured contrast agrees well with the calculations both 5 mm and 12.5 mm depths, with and without the optic. Contrast with the optic was nearly a factor of 2 higher than without the optic for photons at 27 keV and still a factor of 1.4 higher at 46 keV.

Energy (keV)	Scatter Fraction		
	Without Optic	With Optic	
	Measured	Measured	Calculated
20-25	0.50 ± 0.1	0.11 ± 0.10	0.16
40-45	0.77 ± 0.3	0.41 ± 0.16	0.37
75-80	0.77 ± 0.18	0.61 ± 0.20	0.73

Table II. Measured and calculated scatter fraction with and without the optic at three different input energies for the polymethyl methacrylate pahntom.

B. Imaging detector measurements

I. Scatter fraction with imaging detector

Three different energy regions were obtained by using tube voltages of 25, 45, and 80 kV with 0.21, 2.1, and 4 cm thick aluminum filters. The energies listed in this section refer to input, not detected, photons. The scatter ratios were recorded separately for the three different experiments at the three energy ranges. The scatter fractions for the three different energy ranges are listed in Table II. Note that these values are higher than those of Table I, because they are total scatter at all energies. Also they increase rather than decrease with energy because there is more total scatter detected at all energies for a higher energy input.

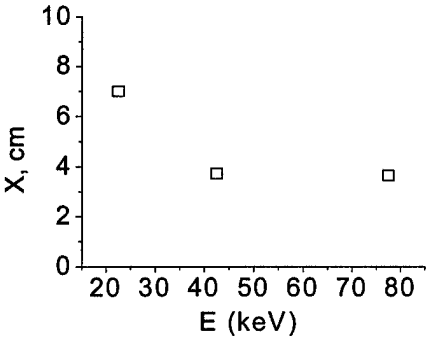

Figure 8. Apparent source location, X versus photon input energy.

The theoretical scatter fraction, calculated using equation 3, is in good agreement with the measured scatter fraction with the optic in Table II. The apparent source location from equation (2), plotted in Figure 8, moves closer to the detector as the input photon energy rises, consistent with the increase scatter fraction. Scatter fraction was reduced by a factor of 4 and 2 for PMMA at 20-25 and 40-45 keV respectively, with the optic.

II. *Contrast with imaging detector*

To measure the contrast, the transmitted intensity through the holes and through the surrounding area was recorded using the Fuji image plate. The measured and calculated contrast for PMMA phantom are shown in Figure 9. The measurement agrees with calculations, showing that the imaging detector can be employed with a selected input spectra to measure the total scatter. The contrast was enhanced by a factor of 1.7 with optic for the input energy range 40-45 keV and 1.5 at 75-80 keV.

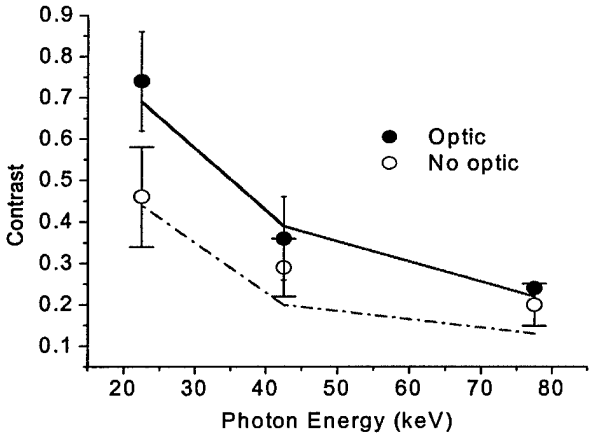

Figure 9. Contrast versus input energy for hole depth 30 mm. The solid and dotted lines are calculations for the optic and no optic case, respectively.

6 Comparison of Energy Specific and Imaging scatter fraction Data

It would be desirable to compare the scatter fraction data taken with a broadband input and the energy sensitive detector to that taken with a narrow-band input and the imaging detector. Since multiple Compton scattering changes the energy of the x ray, one cannot directly compare the results for 40-45 keV input from section 5-B to the 40 keV output data in section 5-A. However it is possible to estimate what the results would have been for a broadband input with broadband capture for both measurements. To model a broadband input, the narrow-band input data of section 5-B was scaled according to the actual input spectrum of section 5-A. Because that spectrum only ranges to 46 keV, it is modeled using only two blocks of the three, representing 20-25 and 40-45 keV, as shown in Figure 10. The relative fraction of the input intensity in each of the energy ranges is calculated as

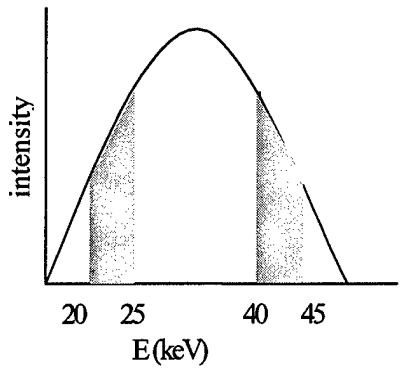

Figure 10. A schematic diagram of selected energy windows.

$$W_1 = \frac{I_1}{I_2 + I_1} \text{ and } W_2 = \frac{I_2}{I_1 + I_2}, \qquad (6)$$

where

$$I_1 = \int_{20}^{25} I(E)dE \text{ and } I_2 = \int_{40}^{45} I(E)dE, \quad (7)$$

and I (E) is the actual input spectrum. One can normalize the primary intensity as

$$I_P = \sum W_i = 1. \qquad (8)$$

Since $SF_i = \frac{I_{Si}}{I_{Si} + I_{Pi}}$, the scatter intensity in each energy range is

$$I_S = \frac{W_1 SF_1}{1 - SF_1} + \frac{W_2 SF_2}{1 - SF_2}, \qquad (9)$$

where SF_1 is the scatter fraction of the material in the energy range 20-25 keV and SF_2 is the scatter fraction in the range 40-45 keV.

Then the total scatter fraction measured with the imaging plate with a broadband input without the optic would have been

$$SF_B = \frac{I_S}{I_S + I_P} = \frac{W_1 SF_1(1 - SF_2) + W_2 SF_2(1 - SF_1)}{(1 - SF_1)(1 - SF_2) + W_1 SF_1 + W_2 SF_2} = 0.36 \pm 0.10 \qquad (10)$$

For the optic, the total scatter fraction measured with the imaging plate with a broadband input was SF_B=0.2 ± 0.1, giving a scatter reduction of a factor R_B = 1.9 ±0.3. To calculate the same total scatter fraction that would have been measured for the actual broadband input data of section A, weights for each of the output energy intervals in Table were computed for the two block input spectrum of Figure 10. The output primary intensity for the nth energy interval was taken as

$$I_{Pn} = \frac{Q_n e^{-\alpha_n t}}{\sum_i Q_i e^{-\alpha_i t}}, \qquad (11)$$

where Q_i is the input intensity in the ith interval, α_i is the total attenuation coefficient of the material for the ith energy interval, and t is the thickness of the phantom. The scatter intensity for that interval was then calculated as

$$I_{Sn} = \frac{SF_n}{1 - SF_n} I_{Pn} \qquad (12)$$

Then the total primary and scatter intensities due to all the detected energies was taken as the sum of the individual values

$$I_S = \Sigma I_{Sn} \text{ and } I_P = \Sigma I_{Pn}. \quad (13)$$

The total scatter fraction which would have been measured for broadband input data can be calculated from I_s and I_p and is $SF_A = 0.27 \pm 0.03$ without the optic and $SF_{AO} = 0.07 \pm 0.01$ with the optic, for a scatter reduction of $R_B = 4 \pm 0.1$. The two estimates, SF_A and SF_B are in reasonable agreement, and agree within the uncertainty. Differences could be attributed to the error in assigning the weights to the energy ranges from the input spectra, and also from attempting to model broadband 5-50 keV spectra with two blocks from 20-25 and 40-45 keV. Knowledge and comparison of energy specific behavior is essential for predicting performance of imaging systems under varying conditions.

Key Accomplishments

- The Polycapillary tapered optic transmission was very good; 45 % and 32 % at 27 and 45 keV.
- The intensity variation of the output beam was 5% rms.
- Scatter was reduced with tapered optic by a factor of 5 at 20-25 keV and by a factor of 3 at 40-45 keV for the PMMA phantom.
- Contrast was enhanced by a factor of 2 at 20-25 keV detected photons.
- Calculations allow comparison of scatter fraction data taken for an monoenergenic input beam with an imaging detector with broadband input data taken with an energy sensitive detector. These comparison increase confidence in extrapolating system performance for varying radiographic conditions.
- The PI will present mamographic imaging data at SPIE August, 2004.
- The PI developed experience working with the setup for scatter rejection and high contrast imaging, with working with optics manufacturers and measurement systems.
- Imaging training with doubly curved crystal optics.

Reportable Outcomes:

- The PI will be submitting a paper on "Scatter Rejection Contrast Measurement Using Tapered Optic" to the journal of medical physics.
- The previous PI moved from a pure physics to a breast cancer research position.

Conclusions:

Tapered optics demonstrated good scatter rejection and contrast enhancement. Multiple tapers in a multiple-taper optic were measured in preparation for measuring the full optic system. The PI obtained experience in measurements of contrast, scatter and image analysis.

References

[1] C.A. MacDonald and W.M. Gibson, "Applications Requirements Affecting Optics Selection," chapter 35 in M. Bass, ed., **Handbook of Optics, Volume III**, McGraw-Hill 2000.